Volume 59
Number 27
7 April 2023
Pages 3929–4088

ChemComm

Chemical Communications

rsc.li/chemcomm

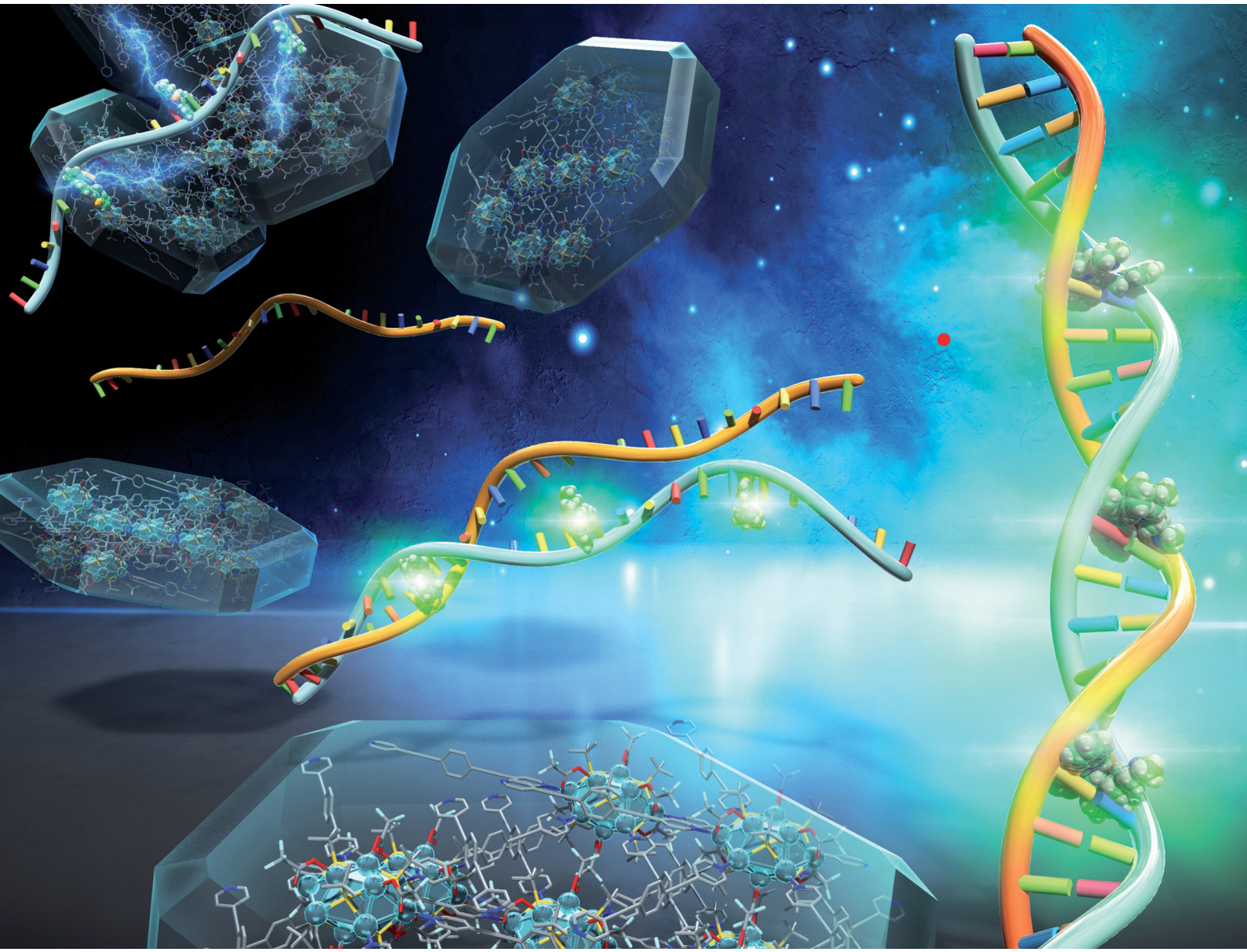

ISSN 1359-7345

ROYAL SOCIETY OF CHEMISTRY

COMMUNICATION

Shuntaro Takahashi, Yuichi Negishi *et al.*

Silver cluster-assembled materials for label-free DNA detection

ChemComm

COMMUNICATION

View Article Online
View Journal | View Issue

Cite this: *Chem. Commun.*, 2023, **59**, 4000

Received 20th December 2022,
Accepted 27th February 2023

DOI: 10.1039/d2cc06933d

rsc.li/chemcomm

Silver cluster-assembled materials for label-free DNA detection†

Saikat Das,[a] Taishu Sekine,[a] Haruna Mabuchi,[a] Sakiat Hossain,[a] Subhabrata Das,[b] Shun Aoki,[c] Shuntaro Takahashi *[b] and Yuichi Negishi *[a]

Herein, we report two newly synthesized silver cluster-assembled materials (SCAMs), $[Ag_{14}(S^tBu)_{10}(CF_3COO)_4(bpa)_2]_n$ (bpa = 1,2-bis(4-pyridyl)acetylene) and $[Ag_{12}(S^tBu)_6(CF_3COO)_6(bpeb)_3]_n$ (bpeb = 1,4-bis(pyridin-4-ylethynyl)benzene) composed of Ag_{14} and Ag_{12} chalcogenolate cluster cores, respectively, bridged by acetylenic bispyridine linkers. The linker structures and electrostatic interaction between positively charged SCAMs and negatively charged DNA confer the SCAMs with the ability to suppress the high background fluorescence of single-stranded (ss) DNA probes with SYBR Green I nucleic acid stain, leading to high signal-to-noise ratio for label-free target DNA detection.

Silver nanoclusters[1,2] have flourished as enticing nanomaterials by virtue of their remarkable photoemission with quantum yields as high as 95%,[3] high catalytic activities,[4] and sensing properties.[5] That said, research on silver nanoclusters has been mostly limited to fundamental studies focusing on the synthesis and isolation of new clusters, resolving their geometric structures, and exploring different surface organic ligands and anion templates as stabilizing/directing agents. The primary concern limiting its applicability is its proneness to oxidization, thereby imparting it with a compromised stability. In light of the foregoing, the transformation of molecular clusters into the extended structure regime have endowed silver cluster-assembled materials (SCAMs)[6] with the advantages of structural diversity, precise designability, and superior stability. SCAMs are crystalline frameworks consisting of polynuclear silver clusters linked together by organic linkers.

The first report on SCAM appeared from Mak and co-workers who exchanged the acetonitrile (CH_3CN) ligands in $[(Ag_{12}(S^tBu)_6(CF_3COO)_6(CH_3CN)_6]\cdot CH_3CN$ cluster with 4,4′-bipyridine (bpy) ligands to construct the two-dimensional (2D) SCAM $[(Ag_{12}(S^tBu)_8(CF_3COO)_4(bpy)_4)]_n$ that exhibited significantly improved stability over one year and 60-fold greater quantum yield.[7] Since then, the library of SCAMs has expanded by combining the diverse geometry and composition of silver cluster nodes with a wide array of organic linkers.[8–12] The combination of silver clusters and organic linkers has not only endowed the SCAMs with augmented stabilities but also with unprecedented performance such as enhanced photoluminescence quantum yields[13–16] and superior photocatalytic bacterial inactivation,[17] among others. However, acetylenic bispyridine linkers have not hitherto been reported to construct the SCAMs. In this study, two novel SCAMs, $[Ag_{14}(S^tBu)_{10}(CF_3COO)_4(bpa)_2]_n$ (hereinafter Ag_{14}bpa) and $[Ag_{12}(S^tBu)_6(CF_3COO)_6(bpeb)_3]_n$ (hereinafter Ag_{12}bpeb) were successfully obtained utilizing two acetylenic linkers, bpa and bpeb (bpa = 1,2-bis(4-pyridyl)acetylene, bpeb = 1,4-bis(pyridin-4-ylethynyl)benzene). Interestingly, the SCAMs, by merit of π-stacking and electrostatic interaction between negatively charged sugar-phosphate backbone of DNA and positively charged cluster assembly, can contribute to fluorescence background quenching of ssDNA probes with fluorescent dye, entailing significant improvement in signal-to-noise ratio (SNR) for label-free DNA detection.

Ag_{14}bpa and Ag_{12}bpeb were prepared in high yields through the one-pot reaction of metal salts (AgS^tBu, CF_3COOAg) and the organic linkers (bpa or bpeb) in a mixture of solvents (acetonitrile/chloroform for Ag_{14}bpa or dimethylacetamide/toluene for Ag_{12}bpeb). First, the reaction took place between AgS^tBu with CF_3COOAg in the aforementioned solvent mixtures. Next, the solutions containing the organic linkers bpa or bpeb were added dropwise. Following solvent removal by slow evaporation, high-quality yellow and colorless single crystals were obtained for Ag_{14}bpa and Ag_{12}bpeb, respectively (ESI† includes full details).

[a] *Department of Applied Chemistry, Faculty of Science, Tokyo University of Science, Kagurazaka, Shinjuku-ku, Tokyo 162-8601, Japan. E-mail: negishi@rs.tus.ac.jp*
[b] *Chemical Materials Development Department, TANAKA KIKINZOKU KOGYO K.K., Tsukuba Technical Center, 22 Wadai, Tsukuba, Ibaraki 300-4247, Japan. E-mail: s-tak@ml.tanaka.co.jp*
[c] *Bio Chemical Development Department, TANAKA KIKINZOKU KOGYO K.K., Hiratsuka Technical Center, 2-73, Shinmachi, Hiratsuka, Kanagawa 254-0076, Japan*

† Electronic supplementary information (ESI) available. CCDC 2231764 and 2231770. For ESI and crystallographic data in CIF or other electronic format see DOI: https://doi.org/10.1039/d2cc06933d

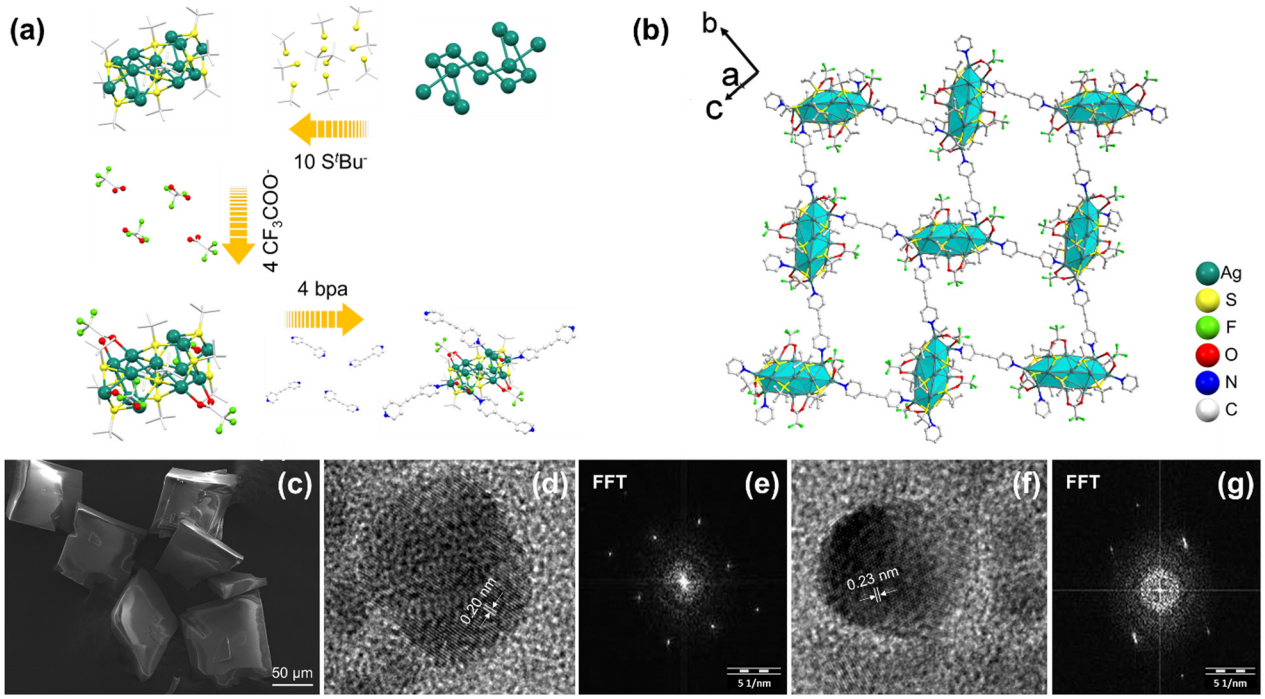

Fig. 1 (a) A step-by-step breakdown of the ligands (S^tBu^- and CF_3COO^-) and bpa linkers connecting to the Ag_{14} core. (b) Extended structure of Ag_{14}bpa. (c) SEM image, (d and f) HR-TEM images of Ag_{14}bpa. (e and g) Fast Fourier transform (FFT) patterns acquired from the areas shown in (d) and (f), respectively.

The structure of Ag_{14}bpa SCAM was determined by single-crystal X-ray diffraction (SCXRD) studies that exhibited monoclinic crystal system, space-group type *C2/c* (Table S1, ESI†). Similar to the situation in Ag_{14}apy,[15] the core of the Ag_{14} cluster in Ag_{14}bpa adopts the shape of a slightly distorted ortho-bielongated square pyramid (Fig. S1, ESI†) in which the Ag5 atoms are located at the apical sites (Fig. S2, ESI†) and the Ag_{14} core is held by $Ag^I\cdots Ag^I$ argentophilic interactions (2.92–3.22 Å, Table S2, ESI†), longer than the Ag–Ag bond length (2.89 Å) of bulk silver,[18] but shorter than the sum of two standard Ag^I van der Waals radii (3.44 Å).[19] The Ag_{14} cluster node features eight square faces and eight triangular faces and is stabilized by ten S^tBu^- and four CF_3COO^- ligands (Fig. 1a). The four μ_3-S (S2, S5) bind to Ag atoms (Ag2, Ag3, Ag4, Ag7) on the square faces with average Ag–S bond length of 2.50 Å (Fig. S2 and Table S3, ESI†) and Ag–S–Ag bond angle in the range of 71.24–128.77° (Fig. S3, ESI†). The two μ_4-S (S4) bind to Ag atoms (Ag1, Ag4, Ag6, Ag7) on the square faces with average Ag–S bond length of 2.65 Å (Fig. S2 and Table S3, ESI†) and Ag–S–Ag bond angle in the range of 64.78–111.47° (Fig. S4, ESI†). The four μ_3-S (S3, S1) bind to Ag atoms (Ag1, Ag2, Ag3, Ag5, Ag6) on the triangular faces with average Ag–S bond length of 2.46 Å (Fig. S2 and Table S4, ESI†) and Ag–S–Ag bond angle in the range of 75.08–124.08° (Fig. S5, ESI†). As can be seen from Fig. S2 and Table S5 (ESI†), the two μ_2-CF_3COO^- (O1, O2) bind to Ag atoms (Ag2, Ag7) on the square faces with average Ag–O bond length of 2.36 Å. The two μ_2-CF_3COO^- (O3, O4) bind to Ag atoms (Ag5, Ag6) on the triangular faces with average Ag–O bond length of 2.40 Å. The Ag_{14} clusters are linked by four bpa linkers with average Ag–N bond length of 2.31 Å (Table S6, ESI†), resulting in a 2D rectangular net with ABA stacking pattern.

Ag_{12}bpeb SCAM crystallizes in the trigonal crystal system with the space group of $R\bar{3}m$ (Table S7, ESI†). The structure of Ag_{12}bpeb is built from the secondary building units (SBUs) $Ag_{12}(S^tBu)_6(CF_3COO)_6$, which are connected to each other through bpeb linkers (Fig. 2a). The cuboctahedron-shaped Ag_{12} core features two equilateral and six isosceles triangles (Fig. S6 and S7, ESI†). In the two equilateral triangles, the average Ag1–Ag1 bond length is 2.96 Å and Ag1–Ag1–Ag1 bond angle is 60° (Fig. S8, ESI†). In the six isosceles triangles, the average Ag1–Ag2 bond length is 3.15 Å, Ag2–Ag1–Ag2 bond angle 74.88°, and Ag1–Ag2–Ag2 bond angle 57.48° (Fig. S9, ESI†). The six μ_4-S (S1) bind to Ag atoms (Ag1, Ag2) with average Ag–S bond length of 2.50 Å and Ag–S–Ag bond angle in the range of 73.48-133.52° (Fig. S10, ESI†). The six μ_1-CF_3COO^- (O2) bind to Ag1 atoms with average Ag–O bond length of 2.41 Å. The Ag_{12} clusters are linked by six bpeb linkers with average Ag–N bond length of 2.29 Å to afford a high-symmetry extended 2D ***hxl*** net that displays the ABCA stacking pattern.

The powder X-ray diffraction (PXRD) patterns of Ag_{14}bpa and Ag_{12}bpeb are in good agreement with the simulated patterns, indicative of the phase purity of the SCAMs (Fig. S11 and S12, ESI†). Scanning electron microscopy (SEM) and optical microscopy characterization of the SCAMs revealed single crystals with well-defined morphology (Fig. 1c, 2c and Fig. S13, ESI†). The lattice fringes of the SCAMs could be clearly observed from the high-resolution transmission electron microscopy (HRTEM)

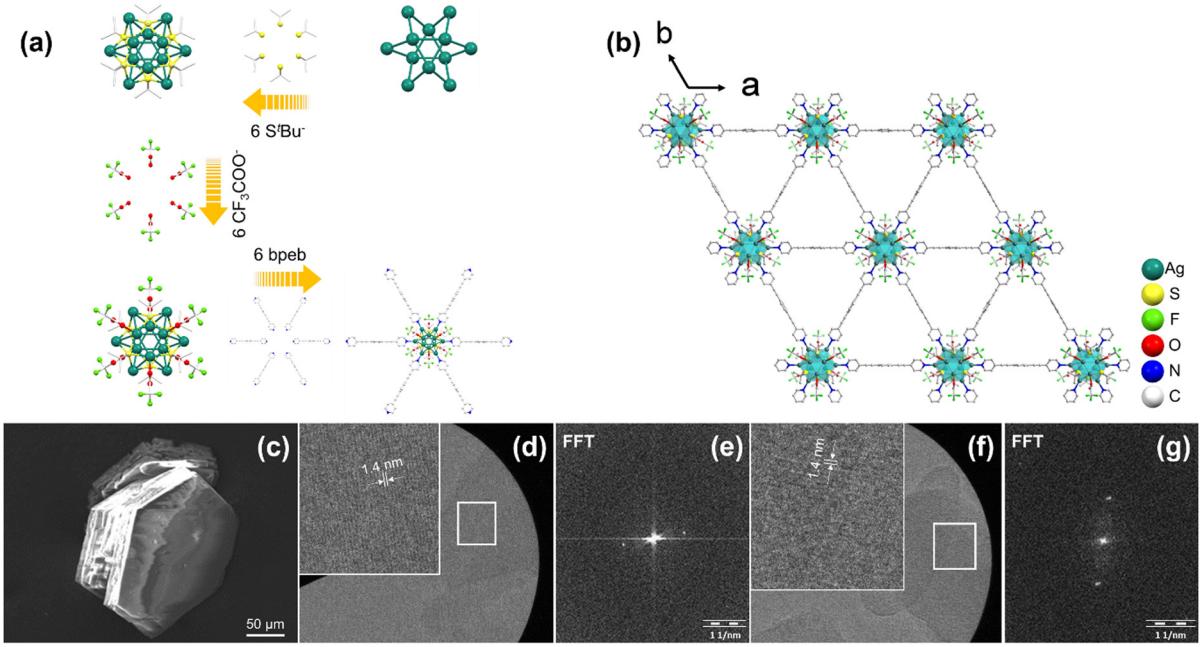

Fig. 2 (a) A step-by-step breakdown of the ligands (S^tBu^- and CF_3COO^-) and bpeb linkers connecting to the Ag_{12} core. (b) Extended structure of Ag_{12}bpeb. (c) SEM image, (d and f) HR-TEM images of Ag_{12}bpeb. (e and g) Fast Fourier transform (FFT) patterns acquired from the areas shown in (d) and (f), respectively.

images (Fig. 1d, f and 2d, f). Thermogravimetric analysis (TGA) showed that the Ag_{14}bpa and Ag_{12}bpeb remained stable up to ~200 °C and 150 °C, respectively (Fig. S14 and S15, ESI†). To assess the chemical stability of Ag_{14}bpa and Ag_{12}bpeb, we immersed the SCAMs in different organic solvents and water. As evident from the PXRD patterns (Fig. S16 and S17, ESI†), the structural integrity of the SCAMs was well-maintained after the treatment.

The unique structural features of the SCAMs intrigued us to explore their potential as label-free DNA sensors. As illustrated in Fig. S20 (ESI†), the DNA detection assay was prepared by hybridizing the probe DNA (40 nM) with the target DNA (40 nM) in 10 mM phosphate buffer (pH 7.4) at 37 °C for 30 min. Subsequently, 0.245 μM SYBR Green I dye was added and incubated at room temperature. Finally, Ag-SCAM (2.0 mg mL^{-1}) was added to achieve the desired concentration. The final mixture was incubated at room temperature for another 30 min, and then centrifuged at 20 000 × *g* for 5 minutes. The supernatant obtained was directly used for fluorescence measurement. The fluorescence measurements were captured with an excitation wavelength of 490 nm, and the emission wavelength was recorded at 521 nm.

Consistent with the literature,[20] the principle of recognition of target DNA goes as (Fig. 3a): the ssDNA probe with fluorescent dye is adsorbed onto the surface of SCAMs, the latter acting as an effective quencher for the fluorescence signal of the former. When the ssDNA probe encounters a target DNA strand, probe hybridization separates the double-stranded DNA from the SCAMs making it inaccessible for quenching, thereby producing signal amplification and high SNR.

As can be seen from Fig. 3b, the SNR of the DNA sensor system is poor when unaccompanied by the SCAMs, the high background fluorescence of ssDNA probes with SYBR Green I nucleic acid stain being the central concern. With the addition of the SCAMs, the background fluorescence shows a steady decline, which in turn enhances the SNR. For Ag_{14}bpa, the SNR reveals a value of *ca.* 42.5 at a Ag_{14}bpa concentration of 5 μg mL^{-1}, a 2.5-fold increase in SNR compared to that before the addition of Ag_{14}bpa. In case of Ag_{12}bpeb, the SNR attained a value of *ca.* 32.5 at a Ag_{12}bpeb concentration of 10 μg mL^{-1}, also a 2.5-fold enhancement in SNR than that prior to the addition of Ag_{12}bpeb. As the concentration of the SCAMs was increased more, the SNR starts declining owing to the adsorption of further double-stranded DNA by the SCAMs.

We attribute the competency of the SCAMs to suppress the high background fluorescence of ssDNA probes with fluorescent dye to the π-stacking and electrostatic interaction. Based on linker structures, the SCAMs reveal a π-stacked conformation (Fig. 3c). We also tested the zeta potentials of Ag_{14}bpa and Ag_{12}bpeb with and without ssDNA probe and SYBR Green I that elucidated the negatively charged backbone of DNA and positively charged cluster assembly (Fig. 3d).

To conclude, Ag_{14} and Ag_{12} chalcogenolate cluster cores were successfully reticulated with acetylenic bispyridine linkers into extended frameworks. We also developed a simple and label-free assay for HIV-1 DNA detection utilizing a DNA probe to hybridize with target DNA sequences and the silver cluster-based frameworks as quencher to diminish the high background fluorescence of ssDNA probes with SYBR Green I nucleic acid stain. This work could chart the way towards harnessing

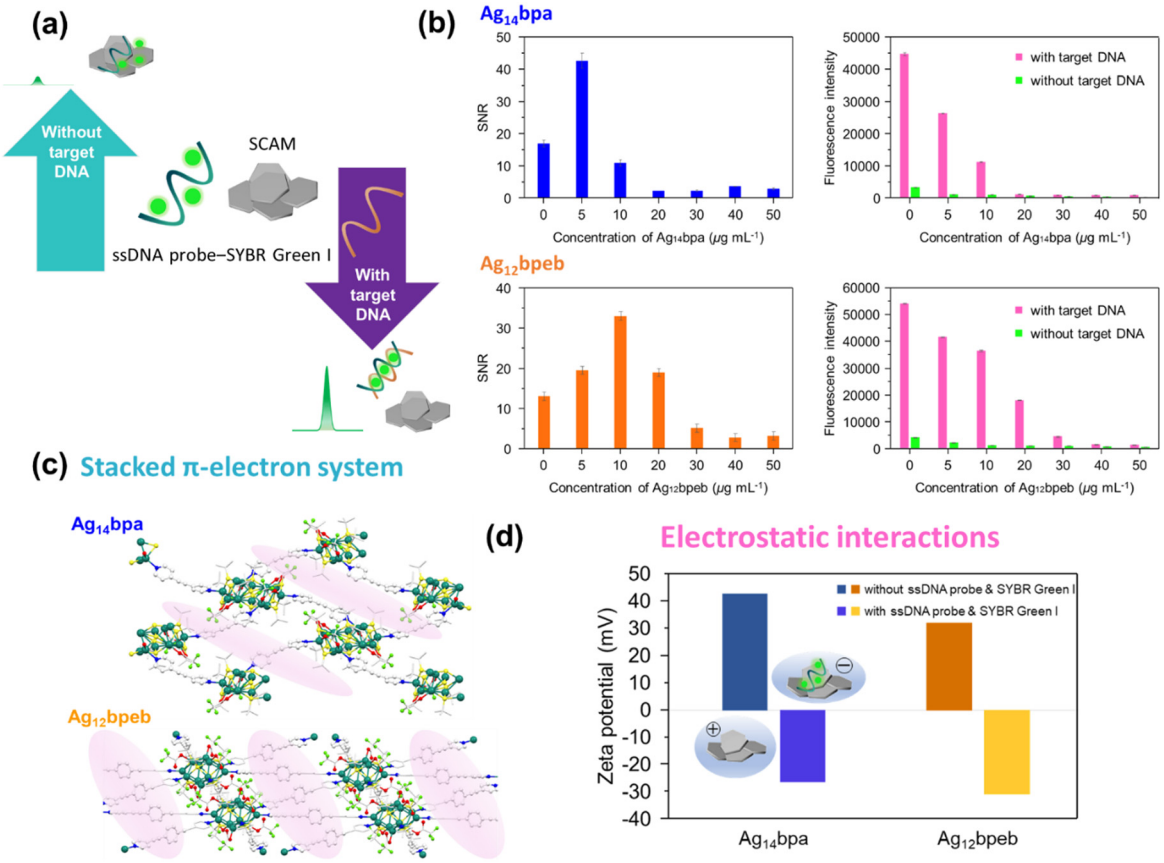

Fig. 3 (a) Label-free approach to target DNA detection using SCAMs, (b) (left) signal-to-noise ratios (SNR) with varying concentration of the SCAMs, and (right) fluorescence intensity of ssDNA probes with SYBR Green I nucleic acid stain *versus* concentration of the SCAMs. (c) π–π stacking system of Ag_{14}bpa and Ag_{12}bpeb. (d) Zeta potential measurements of Ag_{14}bpa and Ag_{12}bpeb with and without ssDNA probe and SYBR Green I.

cluster-assembled materials in DNA-based diagnostics and molecular biology.

Conflicts of interest

There are no conflicts to declare.

Notes and references

1 J. Yang and R. Jin, *ACS Mater. Lett.*, 2019, **1**, 482–489.
2 Y.-P. Xie, Y.-L. Shen, G.-X. Duan, J. Han, L.-P. Zhang and X. Lu, *Mater. Chem. Front.*, 2020, **4**, 2205–2222.
3 Z. Han, X.-Y. Dong, P. Luo, S. Li, Z.-Y. Wang, S.-Q. Zang and T. C. W. Mak, *Sci. Adv.*, 2020, **6**, eaay0107.
4 K. Shimizu, M. Nishimura and A. Satsuma, *ChemCatChem*, 2009, **1**, 497–503.
5 X. Shen, X. Yang, C. Su, J. Yang, L. Zhang, B. Liu, S. Gao, F. Gai, Z. Shao and G. Gao, *J. Mater. Chem. C*, 2018, **6**, 2088–2094.
6 A. Ebina, S. Hossain, H. Horihata, S. Ozaki, S. Kato, T. Kawawaki and Y. Negishi, *Nanomaterials*, 2020, **10**, 1105.
7 R.-W. Huang, Y.-S. Wei, X.-Y. Dong, X.-H. Wu, C.-X. Du, S.-Q. Zang and T. C. W. Mak, *Nat. Chem.*, 2017, **9**, 689–697.
8 Y.-H. Li, R.-W. Huang, P. Luo, M. Cao, H. Xu, S.-Q. Zang and T. C. W. Mak, *Sci. China: Chem.*, 2019, **62**, 331–335.
9 X.-H. Ma, J.-Y. Wang, J.-J. Guo, Z.-Y. Wang and S.-Q. Zang, *Chin. J. Chem.*, 2019, **37**, 1120–1124.
10 C.-H. Gong, Z.-B. Sun, M. Cao, X.-M. Luo, J. Wu, Q.-Y. Wang, S.-Q. Zang and T. C. W. Mak, *Chem. Commun.*, 2022, **58**, 9806–9809.
11 Z. Wei, X.-H. Wu, P. Luo, J.-Y. Wang, K. Li and S.-Q. Zang, *Chem. – Eur. J.*, 2019, **25**, 2750–2756.
12 J.-J. Zhu, P. Hu, K.-K. Zhou, B. Li and T. Zhang, *Dalton Trans.*, 2017, **46**, 6663–6669.
13 Y.-M. Wang, J.-W. Zhang, Q.-Y. Wang, H.-Y. Li, X.-Y. Dong, S. Wang and S.-Q. Zang, *Chem. Commun.*, 2019, **55**, 14677–14680.
14 M. I. Rogovoy, A. S. Berezin, D. G. Samsonenko and A. V. Artem'ev, *Inorg. Chem.*, 2021, **60**, 6680–6687.
15 A. K. Das, S. Biswas, A. Thomas, S. Paul, A. S. Nair, B. Pathak, M. S. Singh and S. Mandal, *Mater. Chem. Front.*, 2021, **5**, 8380–8386.
16 X.-H. Wu, P. Luo, Z. Wei, Y.-Y. Li, R.-W. Huang, X.-Y. Dong, K. Li, S.-Q. Zang and B. Z. Tang, *Adv. Sci.*, 2019, **6**, 1801304.
17 M. Cao, S. Wang, J.-H. Hu, B.-H. Lu, Q.-Y. Wang and S.-Q. Zang, *Adv. Sci.*, 2022, **9**, 2103721.
18 C.-G. Shi, J.-H. Jia, Y. Jia, G. Li and M.-L. Tong, *CCS Chem.*, 2022, DOI: 10.31635/ccschem.022.202201960.
19 H. Schmidbaur and A. Schier, *Angew. Chem., Int. Ed.*, 2014, **53**, 2–41.
20 J. M. Fang, F. Leng, X. J. Zhao, X. L. Hu and Y. F. Li, *Analyst*, 2014, **139**, 801–806.